

Aberystwyth University

Three-dimensional contact of transversely isotropic transversely homogeneous cartilage layers

Vitucci, Gennaro; Mishuris, Gennady

Published in:

European Journal of Mechanics - A/Solids

DOI:

[10.1016/j.euromechsol.2017.04.004](https://doi.org/10.1016/j.euromechsol.2017.04.004)

Publication date:

2017

Citation for published version (APA):

Vitucci, G., & Mishuris, G. (2017). Three-dimensional contact of transversely isotropic transversely homogeneous cartilage layers: A closed-form solution. *European Journal of Mechanics - A/Solids*, 65, 195-204. <https://doi.org/10.1016/j.euromechsol.2017.04.004>

Document License

CC BY-NC-ND

General rights

Copyright and moral rights for the publications made accessible in the Aberystwyth Research Portal (the Institutional Repository) are retained by the authors and/or other copyright owners and it is a condition of accessing publications that users recognise and abide by the legal requirements associated with these rights.

- Users may download and print one copy of any publication from the Aberystwyth Research Portal for the purpose of private study or research.
- You may not further distribute the material or use it for any profit-making activity or commercial gain
- You may freely distribute the URL identifying the publication in the Aberystwyth Research Portal

Take down policy

If you believe that this document breaches copyright please contact us providing details, and we will remove access to the work immediately and investigate your claim.

tel: +44 1970 62 2400

email: is@aber.ac.uk

Accepted Manuscript

Three-dimensional contact of transversely isotropic transversely homogeneous cartilage layers: A closed-form solution

Gennaro Vitucci, Gennady Mishuris

PII: S0997-7538(16)30342-4

DOI: [10.1016/j.euromechsol.2017.04.004](https://doi.org/10.1016/j.euromechsol.2017.04.004)

Reference: EJMSOL 3428

To appear in: *European Journal of Mechanics / A Solids*

Received Date: 17 October 2016

Revised Date: 3 April 2017

Accepted Date: 6 April 2017

Please cite this article as: Vitucci, G., Mishuris, G., Three-dimensional contact of transversely isotropic transversely homogeneous cartilage layers: A closed-form solution, *European Journal of Mechanics / A Solids* (2017), doi: 10.1016/j.euromechsol.2017.04.004.

This is a PDF file of an unedited manuscript that has been accepted for publication. As a service to our customers we are providing this early version of the manuscript. The manuscript will undergo copyediting, typesetting, and review of the resulting proof before it is published in its final form. Please note that during the production process errors may be discovered which could affect the content, and all legal disclaimers that apply to the journal pertain.



Three-dimensional contact of transversely isotropic transversely homogeneous cartilage layers: A closed-form solution.

Gennaro Vitucci^{1,*}, Gennady Mishuris^{1,*}

^a*Department of Mathematics, IMPACS, Aberystwyth University, Aberystwyth, Wales, UK*

Abstract

Inhomogeneity and anisotropy play a crucial role in attributing articular cartilage its properties. The frictionless contact involves two thin biphasic transversely isotropic transversely homogeneous (TITH) cartilage layers firmly attached onto rigid substrates and shaped as elliptic paraboloids of different radii. Using asymptotic techniques, a solution to the deformation problem of such material has been recently obtained extending previous ones referred to homogeneous materials. The layer itself is thin in comparison with the size of the contact area and the observed time is shorter than the hydrogel characteristic time. The emerging three-dimensional contact problem is solved in closed-form and numerical benchmarks for constant and oscillating loads are given. The results are shown in terms of contact pressure and approach of the bones. The latter is derived to be directly proportional to the contact area. Existing experimental data are reinterpreted in view of the current model formulation. Comparisons are made with existing solutions for homogeneous biphasic materials in order to underline the functional importance of inhomogeneity in spreading the contact pressure distribution across the contact area. Particular attention is paid to the applicability of the retrieved formulas for interpreting measurements of *in vivo* experiments. Future directions are also prospected.

Keywords:

articular cartilage, contact mechanics, transversely isotropic transversely homogeneous, biphasic biological tissue, asymptotic analysis

1. Introduction

Articular cartilage covers the bones extremities converging into the diarthrodial joints. It performs the task of improving the load transmission cutting down friction and stress peaks. This biological tissue peculiar properties are enhanced by a complex multiphasic structure. The solid phase mainly consists of a porous proteoglycan matrix reinforced by collagen fibers. Their inhomogeneous arrangement across the layer depth causes inhomogeneity and anisotropy both in the stiffness and permeability of the solid skeleton. The voids are saturated an by interstitial fluid which is chiefly composed of water and mobile

*Corresponding author at: room 5.03, Physical Sciences, Aberystwyth University, SY23 3BZ Aberystwyth, Wales, UK

Email address: gev4@aber.ac.uk (Gennaro Vitucci)

ions causing electro-chemo-mechanical interactions (e.g. Lai et al. (1991); Loret and Simões (2007)). Understanding the behavior of such an intricate system has long stimulated scientific research because of the necessity of patient specific diagnosis of degenerative pathologies, such as osteoarthritis, and challenging tissue engineering for adequate replacement (e.g. see Ateshian et al. (2015); Hollister (2005) for literature review).

A steady progress in computational power encouraged to build biphasic and triphasic fiber-reinforced material models and to search for solutions by use of finite element analysis (Li et al. (1999); Korhonen et al. (2003); Placidi et al. (2008); Görke et al. (2012)). The correspondence between triphasic and biphasic models and the possible occurring difficulties have been discussed in Ateshian et al. (2004); Meng et al. (2017). The thinness of the cartilage layers with respect to the size of the bones and contact area, though, may give origin to ill-conditioning, numerical instability and high computational costs due to the necessity for highly refined meshes in the vicinity of the layer (Wilson et al. (2005)). Because of this, analytical formulations still benefit of popularity in the field and are, so far, able to include a wide range of nonlinear effects such as strain-dependency of the material properties and tension-compression nonlinearity (e.g. Mow et al. (1980); Soltz and Ateshian (2000); Holzapfel and Ogden (2015)).

The present work inserts in the discussion about how to analytically solve the contact problem of two biphasic layers attached onto rigid substrates. It is done using an asymptotic approach which enables to retrieve closed-form solutions with the advantage of easily analyzable formulas (Argatov and Mishuris (2016)). The studies published so far attain to the cartilaginous material modeled first as isotropic homogeneous (Ateshian et al. (1994)), later as homogeneous but transversely isotropic (Argatov and Mishuris (2015)). Speaking of the utilized geometry, the solution provided in Ateshian et al. (1994) regarded identical spherical surfaces and it was extended to two different radii spheres in Wu et al. (1996, 1997). A new progress was aimed in Argatov and Mishuris (2011) by the introduction of elliptic paraboloids resulting in elliptical contact areas. Nevertheless the importance of inhomogeneity in the material property distribution across the thickness has been widely explored as a crucial factor in improving superficial fluid support, thus protecting the tissue from damage (Krishnan et al. (2003); Federico and Herzog (2008)). This was the reason for our recent study Vitucci et al. (2016), summarized in Sec. 2, where a special exponential-type inhomogeneity was introduced. It provided, to the best of our knowledge, the first such asymptotic solution to the deformation of an inhomogeneous biphasic layer, whereas studies existed already concerning monophasic layers obtained in the framework of functionally graded materials (Chidlow et al. (2013); Tokovyy and Ma (2015) and literature survey there).

The solution to the contact problem is derived in Sec.3 and some numerical benchmarks are illustrated in Sec.4. The physical bounds for the model parameters are discussed. Geometry, solicitations and material stiffness and permeability are assigned trying to be as realistic as possible in the framework of the model by ample use of available publications. Two load conditions are exemplified, a constant load and a sinusoidal one. In particular, by means of the retrieved formulas, the utilized contact radii are extracted from the experimental measurements on human tibiofemoral joints provided Hosseini et al. (2010). In Sec.5 we draw our conclusions on some aspects which suggest how inhomogeneity turns favorable for this specific biological tissue and on the applicability and limitations of the current model. The need for data which can reveal crucial for mechanics scientists in order to provide effective

54 diagnosis tools are also remarked.

55 2. Model and statement of the contact problem

56 The contact of thin cartilaginous layers can not be tackled using an Hertzian approach
 57 mainly for two reasons: the material is not constituted of a single phase and, perhaps even
 58 more critically, the assumption of contacting half spaces is dramatically violated. Because
 59 of that, the inquiry for analytical solutions is commonly responded by using transmission
 60 conditions based on the simplification that the layer thickness is asymptotically small and
 61 its stiffness is much smaller than the underlying bone. The procedure, surveyed by Argatov
 62 and Mishuris (2016), is regardless of the constitutive laws of the material and of the contact
 63 model and consists in: first solving the deformation problem for an infinitely extended thin
 64 layer to which the same boundary conditions are assigned on the two surfaces but the load
 65 kept general as in Barry and Holmes (2001); then making use of it for coupling two layers
 66 in contact as in Ateshian et al. (1994); Yang (2006).

67 In our recent work Vitucci et al. (2016), the deformation problem for a thin biphasic
 68 transversely isotropic, transversely homogeneous (TITH) biphasic layer was studied. An
 69 infinitely extended thin layer, firmly attached along one face, was loaded perpendicularly to
 70 the opposite one. The fluid flow, whose filtration through the porous matrix was regulated
 71 by the three-dimensional form of Darcy's law, was constrained by the two layer faces by
 72 imposing null fluid pressure derivative there. At the top surface the absence of friction
 73 was enforced via setting zero shear strain in the solid matrix. The initial conditions on
 74 deformation and fluid pressure until the moment when the load is applied were set also
 75 to zero. The solid matrix was considered linear elastic and the interstitial fluid inviscid,
 76 given that the low permeability causes the friction drag to be dominant with respect to the
 77 viscous flow: due to the low permeability of the tissue, the relative velocity of the fluid
 78 through the solid structure makes the inertia terms play no role in the deformation process
 79 under common solicitations as justified also in Holzapfel and Ogden (2016); Klika et al.
 80 (2016). The governing partial differential equations were thus led back to the classical
 81 mixture theory for biphasic poroelasticity as originally derived in Mow et al. (1980). The
 82 solid matrix constitutive law is described by the stiffness matrix

$$\mathbf{A}(z) = \begin{bmatrix} A_{11} & A_{12} & A_{13} & & & \\ A_{12} & A_{11} & A_{13} & & & \\ A_{13} & A_{13} & A_{33} & & & \\ & & & 2A_{44} & & \\ & & & & 2A_{44} & \\ & & & & & 2A_{66} \end{bmatrix}, \quad (1)$$

83 whose components vary through the local depth-coordinate $z \in [0, 1]$ from the surface to
 84 the substrate. Also the diagonal permeability tensor was considered TITH of components
 85 $\text{diag}(\mathbf{K}(z)) = [K_1, K_1, K_3]$. A special exponential inhomogeneity was allowed:

$$\begin{aligned} A_{33} &= a_{33}e^{2\gamma z}, & A_{44} &= a_{44}e^{\alpha z}, & A_{13} &= a_{13}e^{\alpha_{13}z}, \\ K_3 &= k_3e^{-2\gamma z}, & K_1 &= k_1e^{-\gamma_1 z}. \end{aligned} \quad (2)$$

According to it, in spite of an arbitrary exponential variation of every component, A_{33} and K_3 are linked through $\gamma > 0$, thus let respectively increase and decrease of the same ratio across the thickness. The derived relation between the contact pressure P and the surface lowering of the layer surface is expressed via a sum of convolutions in time t as

$$w = \bar{\alpha}_0 \Delta P + \bar{\alpha}_1 \int_0^t e^{\bar{\beta}_1(t-\theta)} \Delta P \, d\theta + \bar{\alpha}_2 \int_0^t e^{\bar{\beta}_2(t-\theta)} \Delta P \, d\theta + \bar{\alpha}_3 \int_0^t \Delta P(\theta) \, d\theta, \quad (3)$$

86 where the operator Δ represents the Laplacian in the plane orthogonal to z . The expression of
87 the coefficients in Eq. (3) as functions of the TITH biphasic material parameters of Eq. (2) are displayed in Tab. 2. Such closed-form asymptotic solution was obtained under the conditions

$\bar{\alpha}_0$	$\frac{2 - e^{-\alpha}(\alpha^2 + 2\alpha + 2)}{\alpha^3 a_{44}} h^3$	$\bar{\alpha}_3$	$\frac{1 - e^{-\gamma_1}}{\gamma_1} h k_1$
$\bar{\alpha}_1$	$\frac{a_{13}(\alpha_{13} - \alpha)(1 - e^{\alpha_{13} - \alpha - 2\gamma})}{\alpha a_{44}} h k_3$	$\bar{\beta}_1$	$(\alpha_{13} - \alpha)(\alpha_{13} - \alpha - 2\gamma) \frac{a_{33} k_3}{h^2}$
$\bar{\alpha}_2$	$(\alpha - 2\gamma) \frac{1 - e^{-\alpha}}{\alpha a_{44}} h k_3 a_{33}$	$\bar{\beta}_2$	$\alpha(\alpha - 2\gamma) \frac{a_{33} k_3}{h^2}$

Table 1: Coefficients of the pressure-displacement asymptotic relation in Eq. (3) as functions of the material parameters of Eq. (2) as derived in Vitucci et al. (2016).

88 that the characteristic scale of the phenomenon along the tissue was much bigger than the
89 thickness h itself and that the observed time t was relatively smaller than the hydrogel
90 characteristic time $\tau_{\text{gel}} = h^2/(A_{33}K_3)$. The solution represents the second-order non-trivial
91 terms of the asymptotic expansion of the displacement field with relative accuracy $\mathcal{O}(h^2/a_*^2)$,
92 where a_* is a length characterizing the loaded area with respect to h . Looking at Eq.(3),
93 however, shows that the problem, though not fully dynamic, remains time-dependent in
94 a way similar to viscoelasticity, which was indeed one of the first models of cartilage in
95 Kempson et al. (1971) but that could not distinguish between the stresses of the single
96 phases as discussed by Mak (1986).
97

98 The articular cartilage joint is the zone where two bone heads (1) and (2), coated by thin
99 films of cartilaginous tissue, get in reciprocal contact. Fig. 1 gives an idea of the geometrical
100 changes due to deformation through a finite cross section of the infinitely extended three-
101 dimensional model. The surface displacements $w^{(i)}$ are taken positive if directed toward the
102 respective bones. The bones approach is $\delta_0 = \delta_0^{(1)} + \delta_0^{(2)}$. If the two cartilage layers present
103 constant thickness, the problem is stated as

$$\delta_0 - w^{(1)} - w^{(2)} = x_3^{(1)} - x_3^{(2)}, \quad (4)$$

where the two undeformed surfaces are elliptic paraboloids of equation

$$x_3^{(i)}(x_1, x_2) = \left(\frac{x_1^2}{2R_1^{(i)}} + \frac{x_2^2}{2R_2^{(i)}} \right) (-1)^{(i+1)}. \quad (5)$$

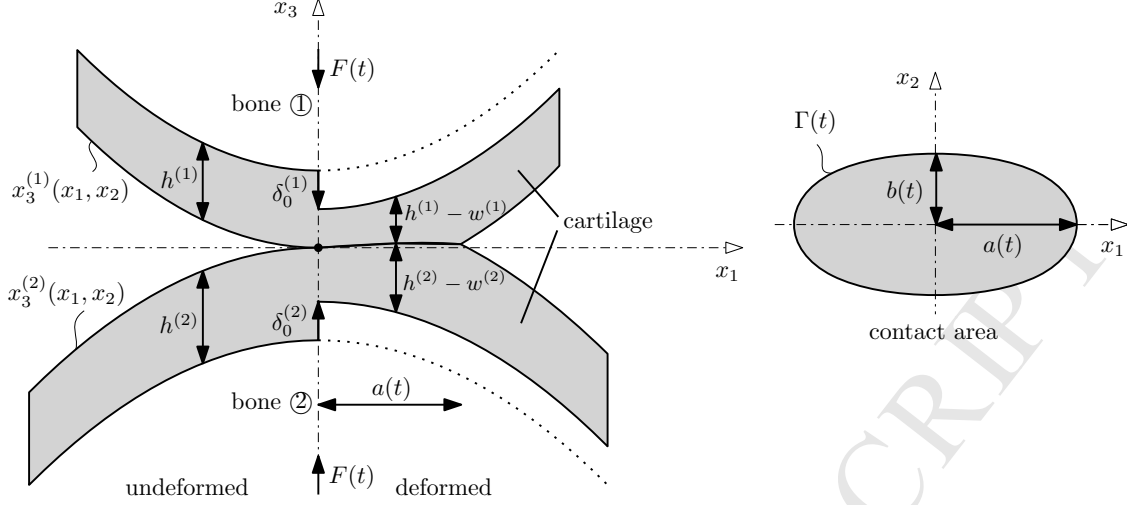


Figure 1: Geometry of the contact problem. On the left-hand side, finite cross section on the plane $x_2 = 0$ of the contact zone between two bone heads covered by constant thickness cartilage (grey) shaped as two elliptical paraboloids. The two sides of the cross section illustrate the geometry before and after the compression caused by the force $F(t)$ (see Eq.(4)). On the right-hand side, the elliptical contact area of major and minor semi-axes $a(t)$ and $b(t)$ (see Eq.(13)).

104 This way the right-hand side of Eq.(4) may be grouped via a function of the planar coordi-
 105 nates only

$$\Phi(x_1, x_2) = \frac{x_1^2}{2R_1} + \frac{x_2^2}{2R_1} \quad (6)$$

106 expressed through the harmonic averages of the radii

$$\frac{1}{R_k} = \frac{1}{R_k^{(1)}} + \frac{1}{R_k^{(2)}} > 0, \quad (7)$$

107 being strictly positive. Later on we associate the index (1) to the convex body lying in the
 108 upper half-space $x_3 > 0$. The studies Argatov and Mishuris (2010a); Rogosin et al. (2016)
 109 offered a solution to the contact problem which accounts also for the displacement component
 110 which is parallel to the contact surface. Despite an increase in computational efforts and
 111 loss of simplicity in the obtained formulas, such rigor did not seem to alter dramatically the
 112 quantitative results within the usual values of the material in exam and it is consequently
 113 neglected in the present work. Substituting the pressure-displacement relation Eq.(3) into
 114 Eq.(4) and multiplying both sides by $m = -(\bar{\alpha}_0^{(1)} + \bar{\alpha}_0^{(2)})^{-1}$ leads to

$$\Delta P(t) + \sum_{j=1}^4 \alpha_j \int_0^t e^{\beta_j(t-\theta)} \Delta P(\theta) d\theta + \alpha_5 \int_0^t \Delta P(\theta) d\theta = m(\Phi - \delta_0), \quad (8)$$

115 once defined $\alpha_5 = -m(\alpha_3^{(1)} + \alpha_3^{(2)})$, $\alpha_j = -m\bar{\alpha}_k^{(i)}$ and the exponents $\beta_j = \bar{\beta}_k^{(i)}$ by re-indexing
 116 $j = i + 2k - 2$ for $k = 1, 2$. It turns useful to introduce the operator \mathcal{G} as

$$\mathcal{G}y(t) = Y(t) = y(t) + \sum_{j=1}^4 \alpha_j \int_0^t e^{\beta_j(t-\theta)} y(\theta) d\theta + \alpha_5 \int_0^t y(\theta) d\theta. \quad (9)$$

117 In view of Eq. (9), Eq. (8) appears now concisely as

$$\mathcal{G}\Delta P(x_1, x_2, t) = m(\Phi(x_1, x_2) - \delta_0(t)). \quad (10)$$

118 The pressure is set to zero outside the contact area. In the case of cartilage it has been
 119 shown that in the superficial area the load is borne mainly by the fluid pressure (Ateshian
 120 et al. (1994); Wu and Herzog (2000); Argatov and Mishuris (2015)), indeed shear strains are
 121 absent because of the absence of friction. It means nullifying also the normal derivative of
 122 the pressure at the border $\Gamma(t)$ of $\omega(t)$ and outside:

$$P = 0, \quad \frac{\partial P}{\partial n} = 0 \quad \text{on} \quad \Gamma(t) \cup \mathbb{R}^2 \setminus \omega(t). \quad (11)$$

123 The total external force $F(t)$ is transmitted through the joint which must be balanced on
 124 both the cartilaginous surfaces by means of the pressure. Specifically:

$$\iint_{\omega(t)} P(x_1, x_2, t) d\omega = F(t). \quad (12)$$

125 Summarizing, the unknowns $\delta_0(t)$, $P(x_1, x_2, t)$ and the contact domain $\omega(t)$ represent the
 126 solution of the described contact problem if: the contact condition is fulfilled via Eq.(10); P
 127 respects the Dirichlet and Neumann boundary conditions Eq.(11) on the moving border of
 128 $\omega(t)$ at any time; the distribution of P results in global balance with the external force $F(t)$
 129 as in Eq.(12).

130 3. Analytical solution

131 The expected contact area between two elliptic paraboloids Eq.(5) of coinciding principal
 132 directions, the Cartesian axes x_1 and x_2 , and pushed toward each other by a force directed
 133 along x_3 and centered at the origin is elliptical with the border description

$$\Gamma(t) : \quad \frac{x_1^2}{a^2(t)} + \frac{x_2^2}{b^2(t)} = 1. \quad (13)$$

134 Consequently, adopting a similar line of reasoning as Argatov and Mishuris (2010b), the
 135 solution to Eq. (10) is searched in the following form: we assume that $\mathcal{G}P(t)$ may be expressed
 136 through the auxiliary variable $p(t)$; then we factorize $p(x_1, x_2, t)$ is the form of a product of
 137 a time function $p_0(t)$ and a part which fulfills *a priori* the boundary conditions Eqs. (11)
 138 on $\Gamma(t)$. Naming $a(t)$ and $b(t)$ respectively the major and minor semi-axes of the elliptical
 139 contact area to determine,

$$p = \mathcal{G}P(x_1, x_2, t) = p_0(t) \left(1 - \frac{x_1^2}{a^2(t)} - \frac{x_2^2}{b^2(t)} \right)^2, \quad (14)$$

140 which transforms to the problem Eq. (10) into

$$\Delta p = m(\Phi - \delta_0). \quad (15)$$

141 Substituting Eq. (14) into Eq. (15), the resulting relation can be split into three simultaneous
 142 conditions by equating the coefficients of the squares of the Cartesian planar coordinates x_1^2 ,
 143 x_2^2 and the remaining constant terms. It will be soon evident how convenient it is to introduce
 144 the ellipse aspect ratio $s(t) = b(t)/a(t)$.

$$\begin{cases} \frac{4p_0}{a^4} \frac{3s^2 + 1}{s^2} = \frac{m}{2R_1}, \\ \frac{4p_0}{a^4} \frac{s^2 + 3}{s^4} = \frac{m}{2R_2}, \\ \frac{4p_0}{a^2} \frac{s^2 + 1}{s^2} = m\delta_0. \end{cases} \quad (16)$$

145 Dividing the first by the second, it turns out that the aspect ratio depends only on the initial
 146 geometry, since it solves

$$3s^4 + \frac{R_1 - R_2}{R_1} s^2 - 3\frac{R_2}{R_1} = 0 \quad (17)$$

147 via the only real positive root

$$s = \sqrt{\frac{R_2 - R_1}{6R_1} + \sqrt{\frac{R_2}{R_1} + \left(\frac{R_2 - R_1}{6R_1}\right)^2}}. \quad (18)$$

148 Such solution is valid for any R_1 and R_2 , if chosen according to Section 2, including the
 149 eventuality that one of the two is negative, which is the common case of a contact between a
 150 concave and a convex bone extremity. Combining for instance the first and the third of the
 151 system (16), $\delta_0(t)$ and $p_0(t)$ are found as power functions of the semi-axis $a(t)$ as follows:

$$\delta_0(t) = \frac{s^2 + 1}{2R_1(3s^2 + 1)} a^2(t); \quad (19)$$

152

$$p_0(t) = \frac{m}{8R_1} \frac{s^2}{3s^2 + 1} a^4(t). \quad (20)$$

153 In view of the latter, Eq. (14) becomes

$$p = \mathcal{G}P(x_1, x_2, t) = \frac{m}{8R_1} \frac{s^2}{3s^2 + 1} \Psi(x_1, x_2, a(t))^2, \quad (21)$$

154 establishing that

$$\Psi(x_1, x_2, a(t)) = a^2(t) - x_1^2 - \frac{x_2^2}{s^2}. \quad (22)$$

155 It remains to enforce the condition Eq. (12) in order to gain the unknown $a(t)$. It is easy
 156 to integrate p over $\omega(t)$ switching to elliptical coordinates with the result:

$$\iint_{\omega(t)} p(x_1, x_2, t) d\omega = \frac{m\pi s^3}{24R_1(3s^2 + 1)} a^6(t). \quad (23)$$

157 Recalling the definition of p in Eq. (14) and moving the time integral operator \mathcal{G} out of
158 the area integral, then the balance condition Eq. (12) appears, leading to

$$a(t) = \left(\frac{24R_1(3s^2 + 1)}{m\pi s^3} \mathcal{G}F(t) \right)^{1/6}. \quad (24)$$

159 In particular, the major semi-axis at the beginning of the loading $a_0 = a(0)$ depends on the
160 geometries and mechanical parameter m of the two contacting bodies and the initial force
161 $F_0 = F(0)$ as

$$a_0 = \left(\frac{24R_1(3s^2 + 1)}{m\pi s^3} F_0 \right)^{1/6} \quad (25)$$

162 and allows to express $a(t)$, $A(t)$ and $\delta_0(t)$ more concisely as

$$\left(\frac{a(t)}{a_0} \right)^6 = \left(\frac{A(t)}{A(0)} \right)^3 = \left(\frac{\delta_0(t)}{\delta_0(0)} \right)^3 = \mathcal{G} \frac{F(t)}{F_0}. \quad (26)$$

163 The asymptotic solution Eq.(3) was obtained under the assumption that the loaded area size
164 is much bigger than the layer thickness, thus F_0 can not be set to zero. The right-hand side
165 of the latter equation results then never indeterminate.

166 In the case of time-independent coefficients α_i and β_i , the operator \mathcal{G} can be inverted as
167 next. Introducing the superscript \sim to indicate the time Laplace transform of parameter σ ,
168 Eq.(9) yields to:

$$\frac{\tilde{y}}{\tilde{Y}} = \left(1 + \sum_{i=1}^4 \frac{\alpha_i}{\sigma - \beta_i} + \frac{\alpha_5}{\sigma} \right)^{-1} = \sigma \frac{\mathcal{P}_n(\sigma^4)}{\mathcal{P}_d(\sigma^5)} = \sigma \sum_{i=1}^5 \frac{B_i}{\sigma - \bar{\sigma}_i}, \quad (27)$$

169 being $\bar{\sigma}_i$ and B_i the poles and the residues of the polynomial fraction $\mathcal{P}_n/\mathcal{P}_d$. The remainder
170 is surely zero because $\deg \mathcal{P}_n < \deg \mathcal{P}_d$. By applying the convolution theorem, the Laplace
171 inversion of the latter gives

$$\mathcal{G}^{-1}Y(t) = y(t) = \sum_{i=1}^5 B_i Y(t) + \sum_{i=1}^5 \bar{\sigma}_i B_i \int_0^t e^{\bar{\sigma}_i(t-\theta)} Y(\theta) d\theta. \quad (28)$$

172 With the inverse operator in the hand and after the due substitutions in Eq. (21), finally
173 the contact pressure can be obtained. Using the symbol H for the Heaviside step function,
174 for fulfilling the boundary conditions Eq. (11) also outside $\omega(t)$, one can write

$$P(x_1, x_2, t) = \frac{ms^2}{8R_1(3s^2 + 1)} \mathcal{G}^{-1} \Psi^2 H(\Psi), \quad (29)$$

175 where $H(\Psi)$ assumes the value 1 when $\Gamma(t)$ reaches the point of coordinates (x_1, x_2) . In the
176 same way it is possible to trace back the individual surface displacements $w^{(i)}$ substituting

$$\Delta P(x_1, x_2, t) = m\mathcal{G}^{-1}(\Phi(x_1, x_2) - \delta_0(t))H(\Psi) \quad (30)$$

177 coming from Eq. (10) into Eq.(3). The problem stated in Section 2 results then analytically
178 solved for the evolution of the contact domain and the bones approach as well as for the
179 contact pressure distribution through Eqs.(18), (24), (19) and (29). Moreover, the guess of
180 ellipticity of the contact area Eq.(4) is confirmed and in agreement with the previous findings
181 about three-dimensional contact of both single- and biphasic thin layers (e.g. see Dowson
182 and Yao (1994); Hlaváček (2008); Argatov and Mishuris (2011)).

183 4. Numerical benchmarks

184 Let us consider a single cartilaginous tissue to which the constitutive laws Eqs. (1) - (2)
 185 apply. The TITH stiffness matrix components A_{13} , A_{33} , the only ones which contribute
 186 to the asymptotic solution in Vitucci et al. (2016) together with A_{44} , can be rewritten as
 187 functions of the in-plane and out-of-plane Young's moduli E_1 , E_3 and the Poisson ratios ν_1 ,
 188 ν_{13} as follows:

$$A_{13} = \frac{\nu_{13}}{1 - \nu_1 - 2\nu_{13}^2 \frac{E_3}{E_1}} E_3; \quad A_{33} = \frac{1 - \nu_1}{1 - \nu_1 - 2\nu_{13}^2 \frac{E_3}{E_1}} E_3. \quad (31)$$

189 The choice of the material parameters is not completely free though, but bounded by physical
 190 restrictions. Particularly, in order to preserve the solid matrix strain energy positivity, it
 191 was proved by Auld (1973) that, for TITH thin layers, it is required that

$$A_{33} \geq A_{13}, \quad A_{33} \geq \frac{3}{4} A_{44} \geq 0. \quad (32)$$

192 Specific and separate values of ν_{13} and ν_1 for a TITH cartilage layer have not been tradition-
 193 ally investigated, but the experimental studies which characterize the material as biphasic
 194 suggest that the apparent isotropic ratio is relatively small (e.g. see Wang et al. (2003);
 195 Keenan et al. (2009); Chagini and Ferguson (2010)). Therefore we assume for simplicity
 196 that $\nu_1 = \nu_{13} = 0$ within the next benchmarks. It is easy to show that, in such situation,
 197 Eqs.(31), combined with Auld's conditions Eq.(32), shrink to

$$A_{13} = 0, \quad A_{33} = E_3 > 0, \quad A_{33} \geq \frac{3}{4} A_{44} > 0. \quad (33)$$

198 At the same time, in Wu and Herzog (2002); Federico et al. (2005) it was shown the
 199 reason why a typical collagen distribution through the cartilage layer causes E_3 also to grow
 200 towards the tidemark at $z = 1$, where $E_1 > E_3$; vice versa E_1 decreases until it becomes
 201 smaller than E_3 at the tidemark. Since the proteoglycan matrix porosity decreases with
 202 the local coordinate z resulting in an overall increased stiffness in the same direction, the
 203 isotropic Young's modulus at the articular surface is smaller than at the bone attachment.
 204 The setting that we will use, which also accounts for these considerations, reads

$$A_{13} = 0, \quad \gamma = \frac{\log 3}{2}, \quad \alpha = \log 10. \quad (34)$$

205 The reader can notice, looking at Eq.(2), that the shear modulus A_{44} presents a tenfold
 206 increase through the depth similarly as in Buckley et al. (2010), while the axial permeability
 207 K_3 , linked to the axial stiffness inhomogeneity by the parameter γ , is let decrease three times
 208 toward the tidemark. As shown in Federico and Herzog (2008), the planar permeability K_1
 209 is expected to be larger than axial K_3 at the articular surface and vice versa at $z = 0$ as the
 210 fluid flows easier along the prevailing collagen fibers orientation, while the overall equivalent
 211 isotropic $K_{\text{iso}} = (2K_1 + K_3)/3$ steadily grows as a result of the decreased porosity. This
 212 leads us to the choice:

$$k_1 = \frac{4}{3} k_{33}, \quad \gamma_1 = \log 6. \quad (35)$$

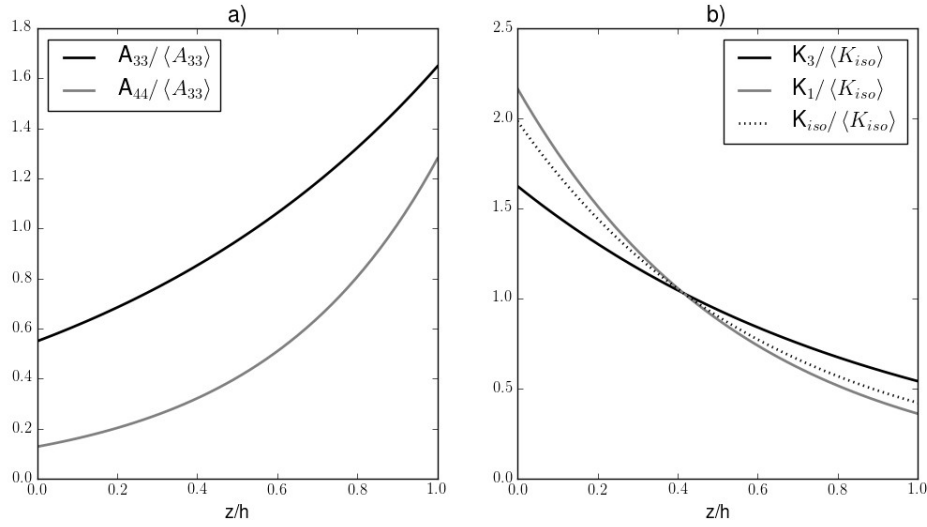


Figure 2: In-depth distribution of material parameters. a) Stiffness matrix elements as multiples of $\langle A_{33} \rangle$. b) Permeability components as multiples of $\langle K_{iso} \rangle$.

213 The material was assigned average typical stiffness values $\langle A_{33} \rangle = 2 \langle A_{44} \rangle = 0.5 \text{MPa}$ (e.g. see
 214 Boschetti et al. (2004)). Furthermore, an isotropic permeability was considered of average
 215 value $\langle K_{iso} \rangle = 2 \cdot 10^{-14} \text{m}^4 \text{N}^{-1} \text{s}^{-1}$ similarly to the findings of Boschetti et al. (2004); Boschetti
 216 and Peretti (2008). The same properties are assigned to all the layers within the following
 217 benchmarks. The resulting distribution of the material parameters through the depth of the
 218 cartilage layer is shown in Fig. 2.

219 Focusing on the tibiofemoral knee joint in extension, it is the locus where the two medial
 220 and lateral femoral condyles - respectively denoted M and L later on - contact the underlying
 221 tibial plateau. The latter is considerably flat at least in the stance contact area, which leads
 222 to choose the curvatures $1/R_1^{(2)} = 1/R_2^{(2)} = 0$. The medial condyle has been observed to be
 223 approximately spherical ((Martelli and Pinskerova (2002); Kim and Suh (2007))) causing an
 224 approximately circular contact area, i.e. $R_1^{(1M)}/R_2^{(1M)} = 1$, $s^{(M)} = 1$. A visual estimate of
 225 the typical lateral contact area detected via magnetic resonance imaging (MRI) published
 226 in Hosseini et al. (2010) reveals a much tapered shape than in the medial compartment with
 227 an aspect ratio of about $s^{(L)} = 0.5$ which indicates $R_1^{(1M)}/R_2^{(1M)} = 7.43$ from Eq. (17), where
 228 the reference axis x_1 is in the sagittal plane, x_2 in the coronal one. Making use of Eq. (19),
 229 one can deduce that the ratio

$$\frac{A(t)}{\delta_0(t)} = \frac{2\pi(3s^2 + 1)}{s^2 + 1} R_1 \quad (36)$$

230 is supposed to be time independent according to our model. Analyzing the results of Hosseini
 231 et al. (2010) in terms of contact area and bones approach, the ratio $A(t)/\delta_0(t)$ presents indeed
 232 appreciably constant slope (see Fig.3), from which we are able to extract the unpublished
 233 size of their 6 patients for both the joint compartments expressed as contact radii. The
 234 retrieved values and standard deviations are illustrated in Fig. 4. The average medial $R_2^{(1M)}$
 235 and lateral $R_2^{(1L)}$ were found to be $30.3 \pm 4.9 \text{mm}$ and $23.9 \pm 5.0 \text{mm}$ with the same level of
 236 uncertainty. The minimum medial radius, in the coronal plane, resulted then approximately

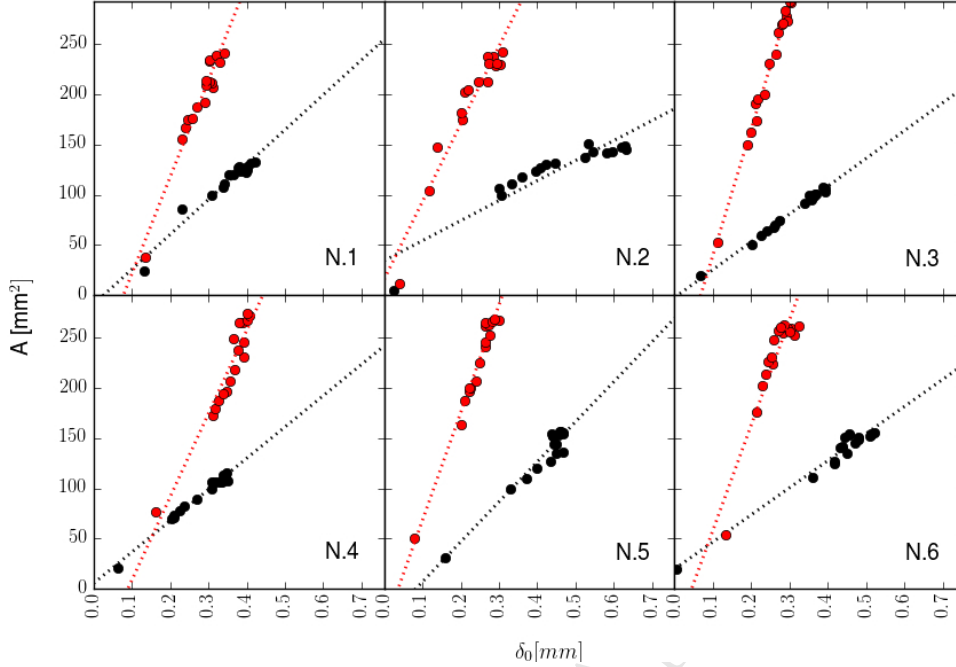


Figure 3: Linear dependency of $A(t)$ and $\delta_0(t)$ observed in the results published in Hosseini et al. (2010). Six human tibiofemoral joints were loaded *in vivo* and the contact area and bones approach were measured via MRI. Such dependency can be explained by Eq.(36). Points represent the experimental results, dotted lines their linear regression. Black indicates the lateral compartment, red the medial one.

237 27% bigger than the lateral one, which is in good agreement with the findings of Siebold
 238 et al. (2010). The fact that the maximum medial radius, the one in the sagittal plane,
 239 is much bigger and equal to 225.3 ± 36.5 mm agrees with the observation by Martelli and
 240 Pinskerova (2002), where they noticed that, at stance, the medial condyle in such direction
 241 appears very flattened and a precise estimation of the contact radius results difficult. The
 242 two couple of average radii are adopted in the subsequent calculations together with the
 243 average thicknesses $h^{(M)} = 1.3$ mm and $h^{(L)} = 1.6$ mm extracted from Hosseini et al. (2010).

244 First we examine the case of a load deriving from a body weight of 700N at stance (about
 245 the European average according to Walpole et al. (2012)), equally split between the two
 246 knees and distributed for 2/3 and 1/3 respectively on the medial and lateral compartments.
 247 It has been indeed measured that the medial compartment carries a much larger part of
 248 the load (Werner et al. (2005); Halder et al. (2012)). What we want to investigate is how
 249 an inhomogeneous distribution of stiffness and permeability may be able to improve the
 250 cartilage performance with respect to a homogeneous one whose properties present the same
 251 average across the thickness. In a way, how an actual cartilage arranges its mechanical
 252 resources for carrying out its functions. The resulting approach $\delta_0(t)$ in Fig. 5 is compared
 253 with the solution of Argatov and Mishuris (2011) for an isotropic homogeneous cartilage
 254 layer. For both the compartments, despite the initial value is smaller than according to
 255 such solution, δ_0 grows remarkably quicker. Besides, its derivative, at least in first seconds,
 256 decreases much faster, pronouncing such desirable property already addressed in Wu et al.

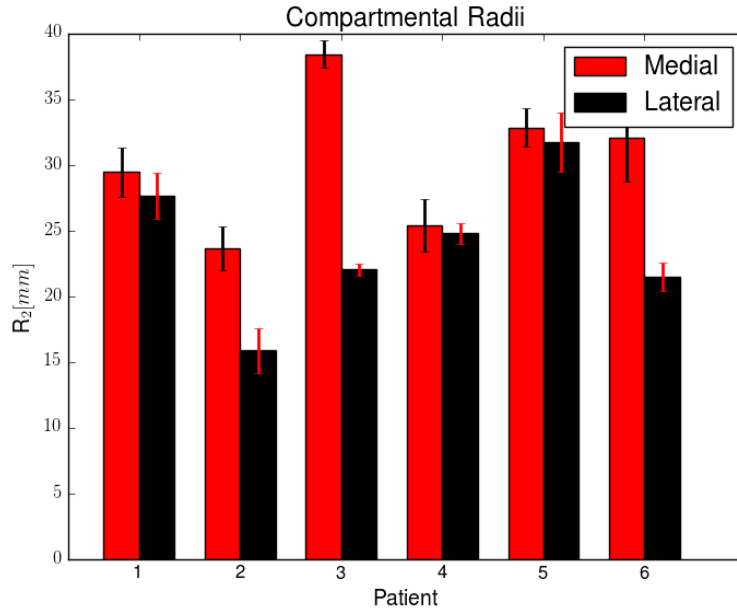


Figure 4: Minimum contact curvature radii R_2 and respective error extracted from the experimental data published by Hosseini et al. (2010) assuming that the aspect ratios of the contact ellipses for the medial and lateral compartments of the tibiofemoral joint are $s^{(M)} = 1$, $s^{(L)} = 0.5$.

(1997). In Fig. 6 we plot the contact pressure along the axis x_1 and its evolution in time. The results, in this case, exhibit not only a quantitative difference, but also a qualitative one. The curves in Fig. 6.a) for the TITH material do not deform homothetically during the expansion of the contact area like the homogeneous material would do, but the novel formula Eq. (29) allow them to change shape by flattening them at the origin. Here the mechanical convenience for the body in developing an inhomogeneous layer appears evident in the sense that, stated that one of the main functions of cartilage is to lower the pressure peaks, such aim is accomplished via a more even distribution of the force inside the contact area together with a faster decrease of the maximum pressure. It is in fact intuitive that it descends from the presence of a compliant zone of high permeability and low stiffness close to the cartilage surface.

The second load condition that we exemplify deals with a sinusoidal force of period 1s, similar to the frequency a normal human gait, and that oscillates on each knee between 0.5 and 1.5 of the same body weight of 700N. The portions absorbed by the two knee compartments stay the same as in the previous benchmark. Fig. 7.a) shows the approach in the first five cycles for both compartments and compares it with the isotropic homogeneous solution homogenized as above. The oscillating part of $\delta_0(t)$ does not indicate a different behavior than the results obtained in Argatov and Mishuris (2011), whereas it is clear that the steadier increase of the average trend is similar to the curves of Fig. 5.a). In the short five cycles interval examined here, the effect discussed with regard to Fig. 5.b) is not observable and in this case the difference between the continuous and dotted lines seems purely an outcome of the larger areas obtained for the isotropic homogeneous material with the particular homogenization criterion chosen in this Section. The oscillating deformation added onto a weakly

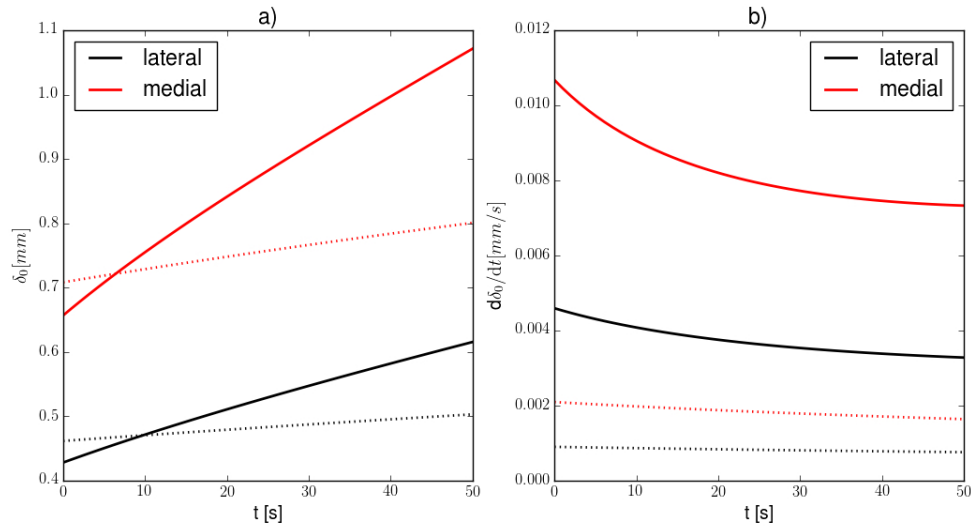


Figure 5: First 50s of a constant load $F = 700\text{N}$. Continuous lines illustrate the results for a TITH material, dotted ones indicate the isotropic homogeneous cartilage behaviour if averaged TITH stiffness and permeability are assigned. The medial compartment bears double as much load as the lateral one. a) Bones approach $\delta_0(t)$. b) Time-derivative of δ_0 .

280 increasing trend shows good agreement with the results of a similar load condition applied
 281 to two identical spherical homogeneous isotropic layers in Wu et al. (2000).

282 5. Discussion and conclusions

283 For the three-dimensional geometry described in Eq.(5), we were able to write the bones
 284 approach, the evolution of the contact area and the corresponding pressure distribution due
 285 to an arbitrary force applied onto the TITH biphasic cartilage layer treated in Vitucci et al.
 286 (2016) (see Eqs.(19), (24), (29)). The solution is retrieved in closed-form and its exact
 287 within the assumptions of the model. The introduction of inhomogeneity and anisotropy
 288 allows to obtain a significantly different lowering of the peak contact pressure and growth
 289 of the contact area with respect to an isotropic homogeneous material whose properties are
 290 simply the average of the TITH one (see examples in Figs. 5,6,7). This proves once more that
 291 the scientist who intends to model the behavior of cartilage needs to pay a great attention
 292 to the interpretation of the material properties provided by experiments. The results are
 293 qualitatively similar to the analytical ones obtained by Chidlow et al. (2013) in the framework
 294 of functionally graded materials when dealing with an inhomogeneous elastic coating on top
 295 of an infinite half-space.

296 It seems remarkable that the ratio of the contact area and the bones approach is pre-
 297 dicted to stay constant in time independently of the applied load as expressed in Eq.(36).
 298 Such proportionality should not be taken for granted even though it arises also in the well
 299 known Hertzian contact theory. Indeed a number of differences exist between our asymp-
 300 totic formulation and the classical one, among which: the nature of our constitutive laws is
 301 biphasic and derives from mixture theory; the Hertzian contact involves half-spaces whereas
 302 ours deals with thin infinite thin layers; Hertz did not impose zero normal derivative to the

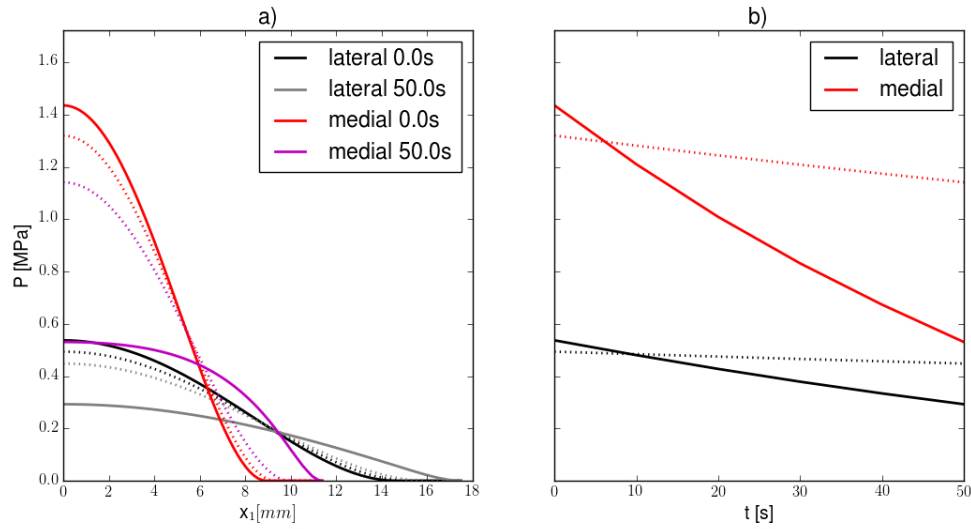


Figure 6: Contact pressure distribution and evolution under constant load. Dotted lines stand for the isotropic homogeneous model. a) Distribution along the axis x_1 containing the major semiaxis $a(t)$ of the elliptical contact area soon after the loading and after 50s. b) First 50s of the pressure in the center of the contact area of coordinates $x_1 = x_2 = 0$.

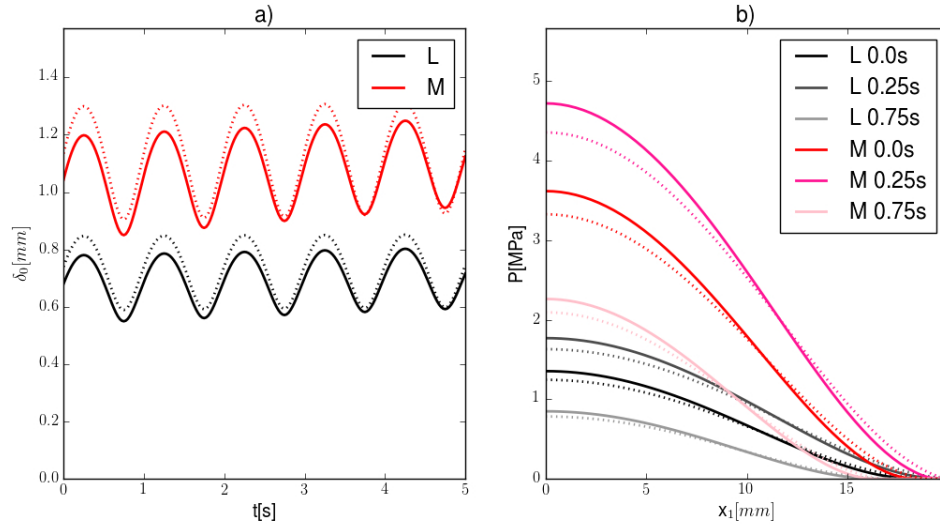


Figure 7: Bones approach and consequent contact pressure profiles under oscillating load. Dotted lines show the response of the isotropic homogeneous material averaged in the sense we discuss in the current section. a) First five cycles of deformations in terms of δ_0 . b) Contact pressure displayed at $t = 0$ and the first maximum and minimum peak of deformation.

303 contact pressure at the border of the contact area. By making use of the latter proportional-
 304 ity, together with assumptions on the ellipticity of the contact areas, it was possible to make
 305 very reasonable guesses about the originating contact radii which were neither published in
 306 the work Hosseini et al. (2010) nor later. The intercepts of the linear regressions in Fig.3
 307 were not zero though and it may derive from initial contact conditions that are different

308 from the ones assumed by our model.

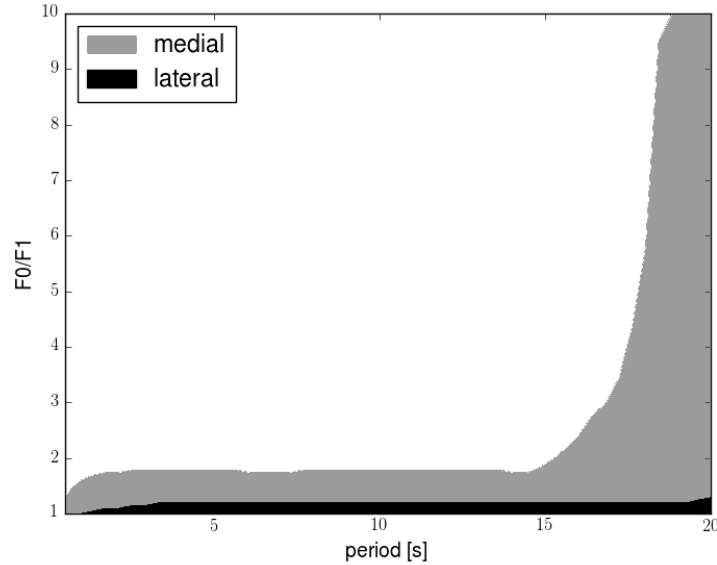


Figure 8: Negative pressure arising under five cycles of loading for different ratios between the constant and oscillatory part F_0 and F_1 of the force and different oscillation periods.

309 All the family of asymptotic solutions Ateshian et al. (1994); Wu et al. (1996, 1997);
 310 Argatov and Mishuris (2011, 2015); Vitucci et al. (2016) do not take into account the de-
 311 pendency of the permeability on the volumetric strain that has been well known since the
 312 study Mow et al. (1980). If this simplification of the equations permits the advantageous
 313 feature of closed-form, easily analyzable solutions, on the other hand it causes the deforma-
 314 tion to emerge unbounded. It can be seen, for instance, in Fig.8 that negative pressure may
 315 arise due to such unboundedness for high oscillating load portions and always for prolonged
 316 load application, visible on the right-hand side of the plot. Such values of the pressure are
 317 obviously unphysical and not acceptable, given that no adhesion is assigned to the layers sur-
 318 faces. On the other hand, that the validity of the proposed approach is constrained to short
 319 time response is part of the model preconditions. Asymptotic formulas of the kind of Eq.(3)
 320 are in fact reliable under the assumption that the considered time is much smaller than the
 321 hydrogel characteristic time $\tau_{\text{gel}} = h^2/(A_{33}K_3)$ which takes the value of about 290s in the
 322 benchmarks of Sec.4. An asymptotic solution which includes the effect of strain-dependent
 323 permeability is currently under investigation and would presumably make the present model
 324 applicable also for later times.

325 The advances in imaging techniques allow nowadays to obtain very detailed measurements
 326 from *in vivo* experiments on articular cartilage. A considerable amount of studies have been
 327 published on the topic, among which Herberhold et al. (1999); Song et al. (2006); Wan et al.
 328 (2008); Li et al. (2008); Bingham et al. (2008); Hosseini et al. (2010); Shin et al. (2011); Chan
 329 et al. (2016). The field looks ready for enhancing early diagnoses of degenerative pathologies
 330 such as osteoarthritis with consequent benefits for the patients. In order to exploit such
 331 technological advantages, though, more extended studies need to be conducted. It would be

332 seriously fruitful for the scientists working on mechanical modeling to see more data provided
 333 in these publications regarding at least the geometry of the contact areas and of the contact
 334 surfaces, the forces applied onto the single articular cartilages. This way a correct modeling
 335 could finally lead to real time analyses and standard procedures.

336 Acknowledgments

337 Gennaro Vitucci and Gennady Mishuris participated in this work under the support
 338 of the European projects, respectively, *FP7-MC-ITN-2013-606878-CERMAT2* and *H2020-*
 339 *MSCA-RISE-2014-644175-MATRIXASSAY*. The authors feel to warmly acknowledge: Ivan
 340 Argatov for all the interesting and fruitful discussions; [the anonymous reviewers because](#)
 341 [answering to their detailed comments has helped to clarify the presentation.](#)

342 Argatov, I., Mishuris, G., 2010a. Axisymmetric contact problem for a biphasic cartilage layer
 343 with allowance for tangential displacements on the contact surface. *European Journal of*
 344 *Mechanics-A/Solids* 29, 1051–1064.

345 Argatov, I., Mishuris, G., 2010b. A closed-form solution of the three-dimensional contact
 346 problem for biphasic cartilage layers. preprint arXiv:1009.4490 .

347 Argatov, I., Mishuris, G., 2011. Elliptical contact of thin biphasic cartilage layers: Exact
 348 solution for monotonic loading. *Journal of biomechanics* 44, 759–761.

349 Argatov, I., Mishuris, G., 2015. *Contact Mechanics of Articular Cartilage Layers*. Springer.

350 Argatov, I., Mishuris, G., 2016. Articular contact mechanics from an asymptotic modeling
 351 perspective: a review. *Frontiers in Bioengineering and Biotechnology* 4, 83.

352 Ateshian, G.A., Chahine, N.O., Basalo, I.M., Hung, C.T., 2004. The correspondence between
 353 equilibrium biphasic and triphasic material properties in mixture models of articular car-
 354 tilage. *Journal of biomechanics* 37, 391–400.

355 Ateshian, G.A., Henak, C.R., Weiss, J.A., 2015. Toward patient-specific articular contact
 356 mechanics. *Journal of biomechanics* 48, 779–786.

357 Ateshian, G.A., Lai, W.M., Zhu, W.B., Mow, V., 1994. An asymptotic solution for the
 358 contact of two biphasic cartilage layers. *Journal of biomechanics* 27, 1347–1360.

359 Auld, B.A., 1973. *Acoustic fields and waves in solids*. Ripol Classic.

360 Barry, S., Holmes, M., 2001. Asymptotic behaviour of thin poroelastic layers. *IMA journal*
 361 *of applied mathematics* 66, 175–194.

362 Bingham, J., Papannagari, R., Van de Velde, S., Gross, C., Gill, T., Felson, D., Rubash,
 363 H., Li, G., 2008. In vivo cartilage contact deformation in the healthy human tibiofemoral
 364 joint. *Rheumatology* 47, 1622–1627.

365 Boschetti, F., Pennati, G., Gervaso, F., Peretti, G.M., Dubini, G., 2004. Biomechanical
 366 properties of human articular cartilage under compressive loads. *Biorheology* 41, 159–166.

- 367 Boschetti, F., Peretti, G.M., 2008. Mechanical properties of normal and osteoarthritic human
368 articular cartilage. *Journal of Biomechanics* 41, S171.
- 369 Buckley, M.R., Bergou, A.J., Fouchard, J., Bonassar, L.J., Cohen, I., 2010. High-resolution
370 spatial mapping of shear properties in cartilage. *Journal of biomechanics* 43, 796–800.
- 371 Chan, D.D., Cai, L., Butz, K.D., Trippel, S.B., Nauman, E.A., Neu, C.P., 2016. In vivo
372 articular cartilage deformation: noninvasive quantification of intratissue strain during joint
373 contact in the human knee. *Scientific reports* 6.
- 374 Chegini, S., Ferguson, S.J., 2010. Time and depth dependent poisons ratio of cartilage
375 explained by an inhomogeneous orthotropic fiber embedded biphasic model. *Journal of*
376 *biomechanics* 43, 1660–1666.
- 377 Chidlow, S., Chong, W., Teodorescu, M., 2013. On the two-dimensional solution of both
378 adhesive and non-adhesive contact problems involving functionally graded materials. *Eu-*
379 *ropean Journal of Mechanics-A/Solids* 39, 86–103.
- 380 Dowson, D., Yao, J., 1994. Elastohydrodynamic lubrication of soft-layered solids at elliptical
381 contacts: part 2: film thickness analysis. *Proceedings of the Institution of Mechanical*
382 *Engineers, Part J: Journal of Engineering Tribology* 208, 43–52.
- 383 Federico, S., Grillo, A., La Rosa, G., Giaquinta, G., Herzog, W., 2005. A transversely
384 isotropic, transversely homogeneous microstructural-statistical model of articular carti-
385 lage. *Journal of biomechanics* 38, 2008–2018.
- 386 Federico, S., Herzog, W., 2008. On the anisotropy and inhomogeneity of permeability in
387 articular cartilage. *Biomechanics and modeling in mechanobiology* 7, 367–378.
- 388 Görke, U.J., Kaiser, S., Bucher, A., Kreißig, R., 2012. A consistent mixed finite element
389 formulation for hydro-mechanical processes in saturated porous media at large strains
390 based on a generalized material description. *European Journal of Mechanics-A/Solids* 32,
391 88–102.
- 392 Halder, A., Kutzner, I., Graichen, F., Heinlein, B., Beier, A., Bergmann, G., 2012. Influence
393 of limb alignment on mediolateral loading in total knee replacement. *The Journal of Bone*
394 *& Joint Surgery* 94, 1023–1029.
- 395 Herberhold, C., Faber, S., Stammberger, T., Steinlechner, M., Putz, R., Englmeier, K.,
396 Reiser, M., Eckstein, F., 1999. In situ measurement of articular cartilage deformation in
397 intact femoropatellar joints under static loading. *Journal of biomechanics* 32, 1287–1295.
- 398 Hlaváček, M., 2008. Elliptical contact on elastic incompressible coatings. *Engineering Me-*
399 *chanics* 15, 249–261.
- 400 Hollister, S.J., 2005. Porous scaffold design for tissue engineering. *Nature materials* 4,
401 518–524.

- 402 Holzapfel, G.A., Ogden, R.W., 2015. On the tension–compression switch in soft fibrous
403 solids. *European Journal of Mechanics-A/Solids* 49, 561–569.
- 404 Holzapfel, G.A., Ogden, R.W., 2016. *Biomechanics: Trends in Modeling and Simulation.*
405 volume 20. Springer.
- 406 Hosseini, A., Van de Velde, S.K., Kozanek, M., Gill, T.J., Grodzinsky, A.J., Rubash, H.E., Li,
407 G., 2010. In-vivo time-dependent articular cartilage contact behavior of the tibiofemoral
408 joint. *Osteoarthritis and cartilage* 18, 909–916.
- 409 Keenan, K.E., Kourttis, L.C., Besier, T.F., Lindsey, D.P., Gold, G.E., Delp, S.L., Beaupre,
410 G.S., 2009. New resource for the computation of cartilage biphasic material properties
411 with the interpolant response surface method. *Computer methods in biomechanics and*
412 *biomedical engineering* 12, 415–422.
- 413 Kempson, G., Freeman, M., Swanson, S., 1971. The determination of a creep modulus
414 for articular cartilage from indentation tests on the human femoral head. *Journal of*
415 *biomechanics* 4, 239–250.
- 416 Kim, S.I., Suh, T.S., 2007. *World Congress of Medical Physics and Biomedical Engineering*
417 *2006: August 27-September 1, 2006 COEX Seoul, Korea.* volume 14. Springer Science &
418 Business Media.
- 419 Klika, V., Gaffney, E.A., Chen, Y.C., Brown, C.P., 2016. An overview of multiphase cartilage
420 mechanical modelling and its role in understanding function and pathology. *Journal of*
421 *the mechanical behavior of biomedical materials* 62, 139–157.
- 422 Korhonen, R.K., Laasanen, M.S., Töyräs, J., Lappalainen, R., Helminen, H.J., Jurvelin,
423 J.S., 2003. Fibril reinforced poroelastic model predicts specifically mechanical behavior
424 of normal, proteoglycan depleted and collagen degraded articular cartilage. *Journal of*
425 *biomechanics* 36, 1373–1379.
- 426 Krishnan, R., Park, S., Eckstein, F., Ateshian, G.A., 2003. Inhomogeneous cartilage prop-
427 erties enhance superficial interstitial fluid support and frictional properties, but do not
428 provide a homogeneous state of stress. *Journal of biomechanical engineering* 125, 569–
429 577.
- 430 Lai, W.M., Hou, J., Mow, V.C., 1991. A triphasic theory for the swelling and deformation
431 behaviors of articular cartilage. *Journal of biomechanical engineering* 113, 245–258.
- 432 Li, G., Wan, L., Kozanek, M., 2008. Determination of real-time in-vivo cartilage contact
433 deformation in the ankle joint. *Journal of biomechanics* 41, 128–136.
- 434 Li, L., Soulhat, J., Buschmann, M., Shirazi-Adl, A., 1999. Nonlinear analysis of cartilage in
435 unconfined ramp compression using a fibril reinforced poroelastic model. *Clinical Biome-*
436 *chanics* 14, 673–682.
- 437 Loret, B., Simões, F.M., 2007. Articular cartilage with intra-and extrafibrillar waters–mass
438 transfer and generalized diffusion. *European Journal of Mechanics-A/Solids* 26, 759–788.

- 439 Mak, A., 1986. The apparent viscoelastic behavior of articular cartilage: the contributions
440 from the intrinsic matrix viscoelasticity and interstitial fluid flows. *Journal of biomechanical engineering* 108, 123–130.
441
- 442 Martelli, S., Pinskerova, V., 2002. The shapes of the tibial and femoral articular surfaces in
443 relation to tibiofemoral movement. *Bone & Joint Journal* 84, 607–613.
- 444 Meng, Q., An, S., Damion, R.A., Jin, Z., Wilcox, R., Fisher, J., Jones, A., 2017. The effect
445 of collagen fibril orientation on the biphasic mechanics of articular cartilage. *Journal of*
446 *the Mechanical Behavior of Biomedical Materials* 65, 439–453.
- 447 Mow, V., Kuei, S., Lai, W., Armstrong, C., 1980. Biphasic creep and stress relaxation
448 of articular cartilage in compression: theory and experiments. *Journal of biomechanical*
449 *engineering* 102, 73–84.
- 450 Placidi, L., Dell’Isola, F., Ianiro, N., Sciarra, G., 2008. Variational formulation of pre-stressed
451 solid–fluid mixture theory, with an application to wave phenomena. *European Journal of*
452 *Mechanics-A/Solids* 27, 582–606.
- 453 Rogosin, S., Mishuris, G., Koroleva, A., Vinakurava, A., 2016. Analysis of the unilateral
454 contact problem for biphasic cartilage layers with an elliptic contact zone and accounting
455 for tangential displacements. *Mathematical Modelling and Analysis* 21, 585–609.
- 456 Shin, C.S., Souza, R.B., Kumar, D., Link, T.M., Wyman, B.T., Majumdar, S., 2011. In
457 vivo tibiofemoral cartilage-to-cartilage contact area of females with medial osteoarthritis
458 under acute loading using mri. *Journal of Magnetic Resonance Imaging* 34, 1405–1413.
- 459 Siebold, R., Axe, J., Irrgang, J.J., Li, K., Tashman, S., Fu, F.H., 2010. A computerized
460 analysis of femoral condyle radii in acl intact and contralateral acl reconstructed knees
461 using 3d ct. *Knee surgery, sports traumatology, arthroscopy* 18, 26–31.
- 462 Soltz, M.A., Ateshian, G.A., 2000. A conewise linear elasticity mixture model for the anal-
463 ysis of tension-compression nonlinearity in articular cartilage. *Journal of biomechanical*
464 *engineering* 122, 576–586.
- 465 Song, Y., Greve, J., Carter, D., Koo, S., Giori, N., 2006. Articular cartilage mr imaging and
466 thickness mapping of a loaded knee joint before and after meniscectomy. *Osteoarthritis*
467 *and cartilage* 14, 728–737.
- 468 Tokovyy, Y., Ma, C.C., 2015. Analytical solutions to the axisymmetric elasticity and ther-
469 moelasticity problems for an arbitrarily inhomogeneous layer. *International Journal of*
470 *Engineering Science* 92, 1–17.
- 471 Vitucci, G., Argatov, I., Mishuris, G., 2016. An asymptotic model for the deformation of
472 a transversely isotropic, transversely homogeneous biphasic cartilage layer. *Mathematical*
473 *Methods in the Applied Sciences* .
- 474 Walpole, S.C., Prieto-Merino, D., Edwards, P., Cleland, J., Stevens, G., Roberts, I., 2012.
475 The weight of nations: an estimation of adult human biomass. *BMC public health* 12, 1.

- 476 Wan, L., de Asla, R.J., Rubash, H.E., Li, G., 2008. In vivo cartilage contact deformation of
477 human ankle joints under full body weight. *Journal of orthopaedic research* 26, 1081–1089.
- 478 Wang, C.C.B., Chahine, N.O., Hung, C.T., Ateshian, G.A., 2003. Optical determination
479 of anisotropic material properties of bovine articular cartilage in compression. *Journal of*
480 *biomechanics* 36, 339–353.
- 481 Werner, F.W., Ayers, D.C., Maletsky, L.P., Rullkoetter, P.J., 2005. The effect of valgus/varus
482 malalignment on load distribution in total knee replacements. *Journal of biomechanics* 38,
483 349–355.
- 484 Wilson, W., Van Donkelaar, C., Van Rietbergen, R., Huiskes, R., 2005. The role of com-
485 putational models in the search for the mechanical behavior and damage mechanisms of
486 articular cartilage. *Medical engineering & physics* 27, 810–826.
- 487 Wu, J., Herzog, W., 2000. On the pressure gradient boundary condition for the contact of
488 two biphasic cartilage layers. *Journal of biomechanics* 33, 1331–1332.
- 489 Wu, J., Herzog, W., 2002. Elastic anisotropy of articular cartilage is associated with the
490 microstructures of collagen fibers and chondrocytes. *Journal of biomechanics* 35, 931–942.
- 491 Wu, J., Herzog, W., Epstein, M., 1997. An improved solution for the contact of two biphasic
492 cartilage layers. *Journal of biomechanics* 30, 371–375.
- 493 Wu, J., Herzog, W., Epstein, M., 2000. Joint contact mechanics in the early stages of
494 osteoarthritis. *Medical engineering & physics* 22, 1–12.
- 495 Wu, J., Herzog, W., Ronsky, J., 1996. Modeling axi-symmetrical joint contact with biphasic
496 cartilage layers—an asymptotic solution. *Journal of biomechanics* 29, 1263–1281.
- 497 Yang, F., 2006. Asymptotic solution to axisymmetric indentation of a compressible elastic
498 thin film. *Thin Solid Films* 515, 2274–2283.

Research highlights

- The cartilage model is a thin biphasic material with transverse and isotropy.
- Two elliptic paraboloids mutually contact in an elliptical area.
- The mathematical novelty is in the first closed-form solution for such problem.
- Existing *in vivo* experimental data are reinterpreted in this new light.